Journal of Particle Science and Technology 8 (2) (2022) 87-94

Ministry of Science, Research & Technology
Iranian Research Organization for Science and Technology (IROST)

Journal of PARTiCLE Science & Technology

JPST

https://jpst.irost.ir

Research paper

Structural and magnetic properties of chemically synthesized yttrium-substituted nickel nanoferrite

Atefeh Azizi Moghaddam, Abdol Mahmood Davarpanahi*

Department of Physics, Faculty of Science, University of Sistan and Baluchestan, Zahedan, Iran

HIGHLIGHTS

- Nanoparticles of $NiY_{2x}Fe_{2-2x}O_4$ with low concentrations of Y^{3+} (x = 0, 0.02, 0.06, and 0.12) were synthesized via the co-precipitation method.
- Different properties of the samples, such as structural and magnetic properties, have been obtained using XRD, FE-SEM, FT-IR, and VSM techniques.
- The Y content was found to have a significant influence on magnetic properties of the Ni-Y ferrites.

GRAPHICAL ABSTRACT

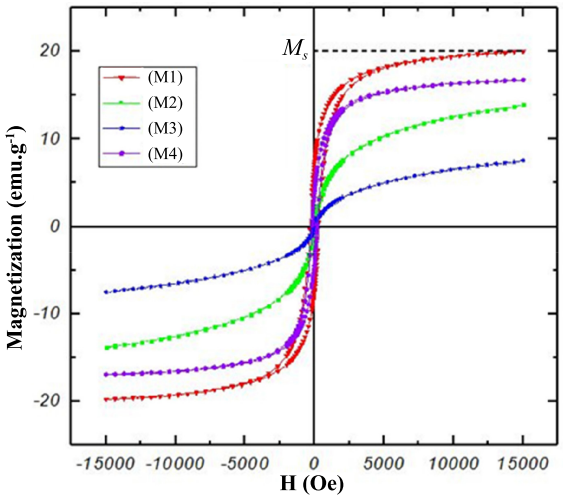

ARTICLE INFO

Article history:

Received 17 January 2023
Revised 5 May 2023
Accepted 8 May 2023

Keywords:

Yttrium-nickel ferrite
Ferromagnetic
Saturation magnetization
Coercivity

DOI: 10.22104/JPST.2023.6077.1222

ABSTRACT

In this paper, yttrium-substituted nickel ferrite ($NiY_{2x}Fe_{2-2x}O_4$) nanostructures were synthesized via the co-precipitation method with different concentrations of yttrium (x = 0.00, 0.02, 0.06, and 0.12 %, where x is the dopant concentration in molar percent) after calcination at 500 ºC. Structural studies of the samples were analyzed using X-ray diffractometry (XRD) technique. XRD results showed that the addition of Y led to an increase in synthesized nanoparticles. Molecular studies have been done using Fourier transform infrared (FT-IR) spectroscopy. FT-IR results showed that the bands at about 550-560 and 433 cm^{-1} are associated with tetrahedral and octahedral Metal–O bonds, respectively. Field emission scanning electron microscopy (FE-SEM) exhibit that adding Y^{3+} ions dopant up to x = 0.06 led to a considerable decrease in the powders' particle size. Adding more dopant up to x = 0.12 led to an amorphous and crystalline phase formation. The size of nanoparticles before substitution estimated from FE-SEM images were 39.49, 36.49, and 50.78 nm, which increased to 63.07, 64.02, and 73.56 nm after the substitution, respectively. The magnetic behavior of the samples was investigated using vibrating sample magnetometry (VSM) at room temperature (RT). VSM results showed that the saturation magnetization and coercivity (H_c) values decreased with the increase of yttrium contents up to x = 0.12. This was referred to as the redistribution of cations on the octahedral bonds.

* *Corresponding author: Tel.: +9854-33446565 ; Fax: +9854-33446565 ; E-mail address: a.m.davarpanah@phys.usb.ac.ir*

1. Introduction

Most ferrites, especially spinel ferrites such as nickel ferrites doped with different elements, have been developed to meet demands in the microwave engineering field [1]. The application of nickel ferrite in the electronic industry is associated with transition metal oxides that can connect to the spinel structure. Nickel ferrite substitutions have been studied extensively due to their wide range of applications [2].

Nickel ferrites have low coercivity and high specific electric resistivity, making them suitable cores for power electronic converters in electronic and communication industries. For example, Salavati-Niasari *et al.* reported that the magnetic properties of nanocrystalline nickel ferrite showed ferromagnetic behavior at room temperature [3]. Manikandan *et al.* showed the hysteresis loop of a soft magnetic nature, and the relevant parameters (M_r, M_s, and H_c) had low values for nickel ferrites, confirming the nature of the material [4].

Khan *et al.* synthesized yttrium-doped nickel ferrite and detected a single-phase cubic spinel structure for $x \leq 0.06$ %; however, for $x \geq 0.08$ %, a dual-phase structure was observed [5]. They found that the lattice constant increased for all doped samples due to the difference between the ionic radius of Fe^{3+} and Y^{3+}, but particle size decreased after yttrium substitution.

Kumbhar *et al.* examined the structural and magnetic properties of thin zinc-nickel ferrite ($Ni_xZn_{1-x}Fe_2O_4$) films with different nickel concentrations (x = 0.00, 0.2, 0.4, 0.6, and 0.8 %) [6]. Using the spray pyrolysis method for thin film deposition, they obtained 28-38 nm crystallites. In addition, they found that the XRD peak intensity increased as the nickel concentration increased. SEM images showed smooth and compact layers composed of spherical particles in the range of 0.12 - 0.22 μm. Finally, the coercivity (H_c) of the ferrite increased while the saturation magnetization (M_s) decreased due to the formation of nanocrystalline grains with more grain boundaries.

Ishaque *et al.* examined the effects of yttrium substitution on FMR line width and magnetic properties of nickel spinel ferrites [7]. They found that the octahedral distribution of cations results in a decrease in saturation magnetization. On the other hand, grain size decreased, and coercivity increased by increasing the yttrium content.

Alves *et al.* investigated the effect of Y^{3+} ions substitution on the structural, optical band-gap, and magnetic properties of cobalt ferrite nanoparticles [8]. They obtained crystallites in the range of 16-35 nm. Cation distribution analysis showed that Y^{3+} ions occupy octahedral B sites, followed by the migration of Co^{2+} ions to tetrahedral A sites, while Fe^{3+} ions distribute both in A and B sites. They also found that the presence of yttrium affects the magnetic properties of the cobalt ferrite. In other words, saturation magnetization and coercivity depend on the temperature and concentration of Y^{3+} ions; saturation magnetization decreased while coercivity increased by increasing the yttrium content, making it a suitable candidate for application in electronic devices, such as magnetic receivers, at room temperature.

Although several researchers have reported Y^{3+} ions substitution to ferrite spinels in the range of $x > 0.2$%, based on the authors' knowledge, the addition of Y in low concentration ranges has not received enough attention in the literature. Therefore, in the present study, diferent amounts of Y^{3+} ions, as a dopant, were added to nickel ferrite ($NiY_{2x}Fe_{2-2x}O_4$, x = 0.00, 0.02, 0.06, and 0.12) during the synthesis process, and the structure, microstructure, molecular, and magnetic properties of the powders were investigated. Another aim of the present research was to investigate yttrium nickel ferrite applications in different fields.

2. Experimental

Nickel ferrite was synthesized via the co-precipitation route using Iron (III) nitrate nonahydrate ($Fe(NO_3)_3.9H_2O$, Merck), Nickel (II) nitrate hexahydrate ($Ni(NO_3)_3.6H_2O$, Merck), and citric acid ($C_6H_8O_7$, Merck) as starting materials with yttrium (III) nitrate tetrahydrate ($Y(NO_3)_3.4H_2O$, Merck) as the dopant source.

First, nickel nitrate, iron nitrate, and yttrium nitrate were dissolved in 100 ml double distilled water with different primary molar concentrations of yttrium nitrate (x = 0.00, 0.02, 0.06, and 0.12), as listed in Table 1. The prepared solutions were then added dropwise to 9 ml citric acid under magnetic stirring. Next, an ammonia solution (NH_4OH) was added dropwise to the original solution under magnetic stirring at 50 °C to obtain a brownish-orange solution. After 1 hour of stirring and heating, a dark brown precipitate was obtained. The precipitate

Table 1. Ferrite nickel samples with different yttrium contents.

Sample	Y Concentration (x, %)	Formula
M1	0.00	$NiFe_2O_4$
M2	0.02	$NiY_{0.04}Fe_{1.96}O_4$
M3	0.06	$NiY_{0.12}Fe_{1.88}O_4$
M4	0.12	$NiY_{0.24}Fe_{1.76}O_4$

was dried at 80 °C in an electric oven for two hours and was then calcined under a nitrogen atmosphere at 500 °C for four hours in an electric furnace. The heating was increased to 500 °C at 20 °C.min^{-1}.

Structural characterization of the samples was performed using X-ray diffraction technique (XRD) (Philips X'Pert X-ray diffractometer with graphite monochromatic Cu-Kα radiation). The mean nickel ferrite crystallite diameter ($d_{Scherrer}$) was determined from the half-height width (β) of the (311) diffraction peak of nickel ferrite using the Scherrer Eq. (1), where θ is the diffraction peak angle [9-11].

$$d_{Scherrer} = 0.9\lambda / \beta\cos\theta \quad (1)$$

The microstructure of the samples was studied using a field emission scanning electron microscope (FE-SEM, MIRA3, TESCAN). Molecular studies were performed using a Fourier transform infrared spectroscope (FT-IR, Bruker TENSOR II) equipped with a platinum ATR accessory with a robust diamond crystal. The magnetic properties of the samples were studied with a vibrating sample magnetometry (VSM, Meghnatis Daghigh Kavir Co., IRAN model) at room temperature. The range of the applied magnetic field was kept at −15 to +15 kOe.

3. Results and discussion

3.1. Structural Studies

Fig. 1 shows the XRD patterns of M1 to M4 powders. As shown, $NiFe_2O_4$ (Trevolite, card no. 00-044-1485) with a spinel structure was formed as the dominant phase for all the samples.

The lattice parameter of $NiFe_2O_4$ was calculated based on the XRD patterns for the (311) diffracted plane using '*d*' spacing using Eq. (2) as follows [10,12]:

$$a = d_{hkl}\,(h^2 + k^2 + l^2)^{1/2} \quad (2)$$

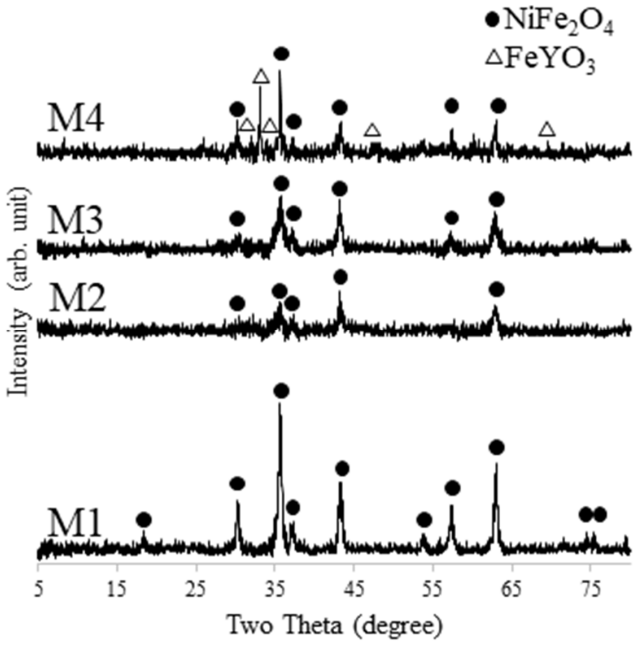

Fig. 1. XRD pattern of the synthesized powders.

The highest peak at (311) confirms the preparation of spinel ferrites [13].

Introducing Y^{3+} ions dopant of x = 0.00 (M1) to x = 0.02 (M2) caused the substitution of Y^{3+} (r = 104 pm) with Fe^{3+} (r = 69 pm) ions, resulting in considerable lattice distortion; consequently, Y^{3+} ions significantly decreased peak intensities. Moreover, the lattice parameter increased from 8.3564 to 8.3612 Å. However, increasing Y^{3+} ions up to x = 0.12 (M4) led to the formation of a minor phase of $FeYO_3$ (card no. 01-086-0170), along with the $NiFe_2O_4$ spinel main phase. The XRD pattern of sample M3 showed narrower peaks than that of M2, and it seems that sample M3 is between the distorted lattice of M2 and the two crystalline phases of M4.

3.2. Molecular studies

FT-IR spectra obtained at room temperature in the wave number range 400 - 4000 cm^{-1} shows the splitting of the two fundamental absorption bands, thereby confirming the completion of the solid-state reaction.

Fig. 2 shows the FT-IR spectra of samples M1-M4. As illustrated, the bands at about 550-560 and 433 cm^{-1} are associated with tetrahedral and octahedral Metal−O bonds, respectively [14-16].

Ferrites are crystallized in a spinel structure. Because the tetrahedral bond length is smaller than the octahedral bond length, the vibration frequency of the tetrahedral

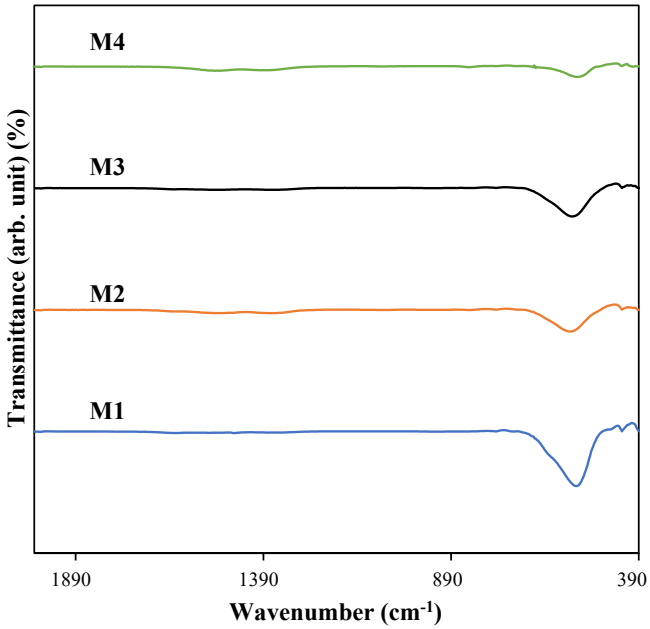

Fig. 2. FT-IR spectra of the synthesized powders.

bond will be higher [17-19].

Fig. 3 shows the FT-IR spectra of the M1 sample (x = 0.00). The insets show the adsorption bands at higher magnification. There are two adsorption bands at 548.27 and 466.37 cm^{-1}, which can be attributed to iron adsorption. The band at 434.10 cm^{-1} can be assigned to nickel adsorption.

Fig. 4 shows the FT-IR spectra of the M2 sample (x = 0.02). It can be seen that the adsorption of iron and nickel have occurred at 573.54 and 435.06 cm^{-1}. However, after yttrium addition, the OH adsorption band shifts to 1371.09 cm^{-1}. Due to its low concentration, no adsorption band is seen for yttrium in this sample.

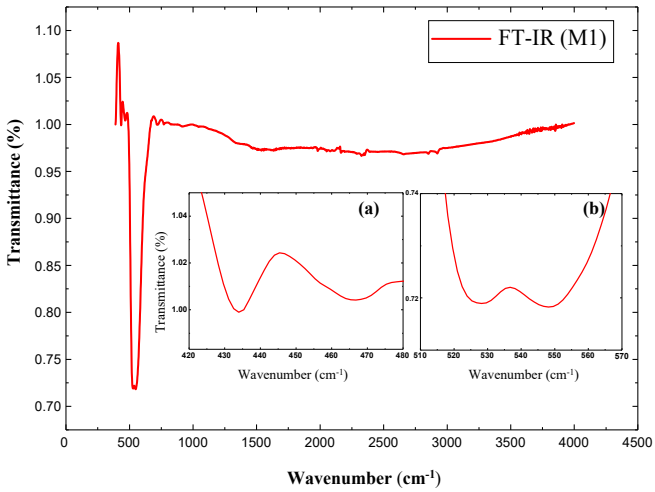

Fig. 3. FT-IR spectra of M1 sample. The insets show adsorption bands at higher magnification: (a) adsorption of nickel and iron at 434.10 and 466.37 cm^{-1}, respectively, and (b) adsorption of iron at 548.27 cm^{-1}.

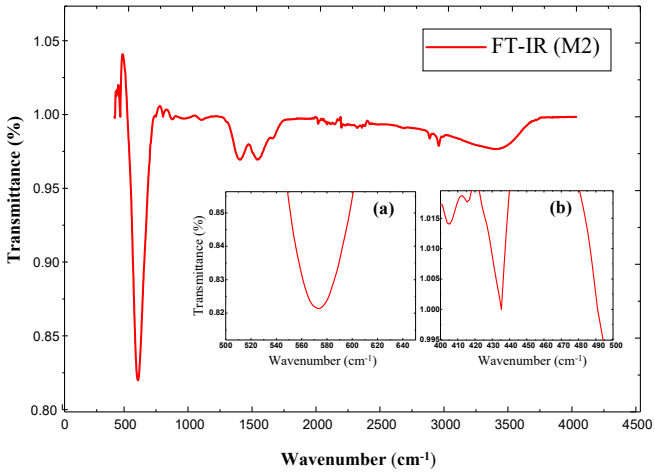

Fig. 4. FT-IR spectra of M2 sample. The insets show adsorption bands at higher magnification: (a) adsorption of iron at 573.54 cm^{-1} and (b) adsorption of nickel at 435.06 cm^{-1}.

Fig. 5 shows the FT-IR spectra of the M3 sample (x = 0.06). It can be seen that the adsorption of iron and nickel have occurred at 566.86 (Fig. 5(a)) and 435.12 cm^{-1} (Fig. 5(b)). Due to its low concentration, this sample also shows no adsorption band for yttrium.

Fig. 6 shows the FT-IR spectra of the M4 sample (x = 0.12). It can be seen that the adsorption of yttrium and nickel has occurred at 404.43 and 435.34 cm^{-1}, respectively (Fig. 6(a)), while the bands at 552.65 and 671.41 cm^{-1} are related to the iron adsorption (Figs. 6(b) and 6(c)). The adsorption band of the OH group with "W-shape" behaviour is also observed at 1500 cm^{-1}.

3.3. Microstructure characterization

Figs. 7(a) - 7(d) show the FE-SEM micrographs of

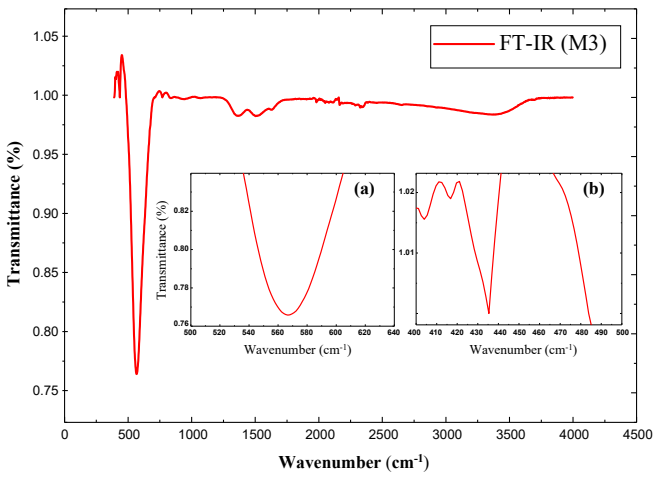

Fig. 5. FT-IR spectra of M3 sample. The insets show adsorption bands at higher magnification: (a) adsorption of iron at 566.86 cm^{-1} and (b) adsorption of nickel at 435.12 cm^{-1}.

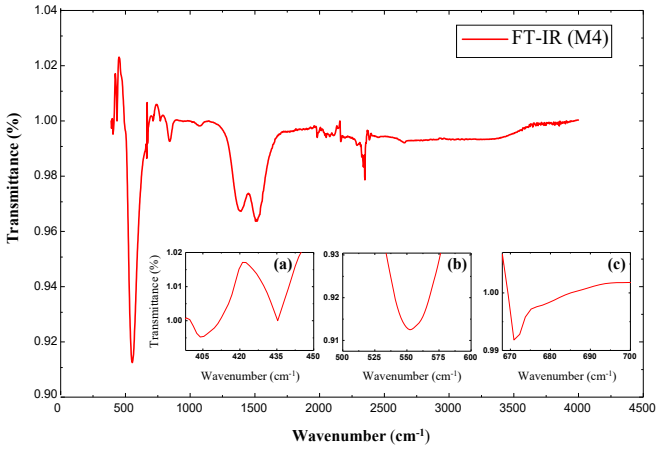

Fig. 6. FT-IR spectra of M4 sample. The insets show adsorption bands at higher magnification: (a) adsorption of yttrium and nickel at 404.43 and 435.34 cm^{-1}, respectively, (b) and (c) adsorption of iron at 552.65 and 671.41 cm^{-1}, respectively.

samples M1 to M4. As illustrated, all samples contained nano-size particles, which were highly agglomerated. Moreover, adding Y^{3+} ions dopant up to x = 0.06 led to a considerable decrease in the powders' particle size (Figs. 7(a): M1, 7(b): M2, 7(c): M3, and 7(d): M4). This is due to the strong distortion of the $NiFe_2O_4$ lattice caused by introducing larger Y^{3+} ions. The larger ions were replaced with iron ions. Adding dopant up to x = 0.12 led to the formation of an amorphous and crystalline phase (Fig. 7(d)). XRD patterns (Fig. 1) revealed that two crystalline phases were obtained: $NiFe_2O_4$ and $FeYO_3$. It seems that Y^{3+} ions caused the formation of an amorphous phase and then preferred to combine with Fe^{3+} and O^{2-} ions to form a $FeYO_3$ phase instead of substituting in the $NiFe_2O_4$. Therefore, amorphous $NiFe_2O_4$ and $FeYO_3$ were synthesized in the M4 sample.

Comparing Fig. 7(d) (M4) with other samples showed different microstructures. The continuous phase, which surrounds the particles, is amorphous.

3.4. Magnetic properties

The magnetic hysteresis loops for samples M1 - M4 are shown in Figs. 8(a) and 8(b). As illustrated, the magnetic hysteresis loop for the M2 sample from which M_s and H_c are determined is 3.904 $emu.g^{-1}$ and 57 Oe, respectively. Thus, it can be concluded that the M2 sample is a soft ferromagnetic material.

Likewise, M_s = 7.522 $emu.g^{-1}$ and H_c = 51.015 Oe can be determined for the M3 sample from Figs. 8(a) and 8(b). According to these values, it can be concluded

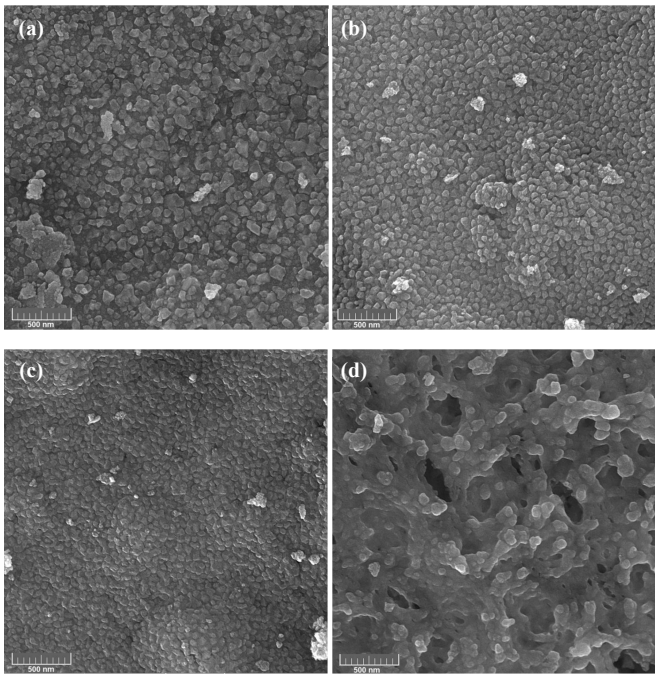

Fig. 7. FE-SEM micrographs of samples (a) M1, (b) M2, (c) M3 and (d) M4.

that the M3 sample, like the M2 sample, is also a soft ferromagnetic material. Therefore, all the samples belong to the family of soft ferrites. As Al-Garalleh *et al.* mentioned, soft magnetic materials are widely used in transformers, multilayer chip inductors, and magnetic recording heads [23]. In addition, ferrite magnetic oxides with favorable magnetic and electrical properties, thermal and chemical stability, and cost-effectiveness have largely replaced metallic magnetic materials in a wide range of technological applications, such as transformer cores, electronic inductors, high-quality filters, and electronic devices.

As seen in Figs. 8(a) and 8(b), M_s and H_c values for the M4 sample are determined as 16.719 $emu.g^{-1}$ and 184.715 Oe, respectively. Thus, similar to the M2 and M3 samples, M4 is also a soft ferromagnetic material. However, when H_c < 200 Oe, the material is a soft ferromagnetic, while for H_c > 200 Oe, the material is considered as a hard ferromagnetic. When the hysteresis curve is "S-shape" and intercepts the origin, the material is considered as superparamagnetic. The M_s and H_c values obtained for M1 to M4 samples are summarized in Table 2.

Sharifitabar *et al.* [21] and Qing Li *et al.* [22] showed that a decrease in particle size led to a decrease in coercivity. However, it seems that in the present study, lattice distortion due to the substitution of Y^{3+} ions (Fig. 1) resulted in a considerable coercivity decline for

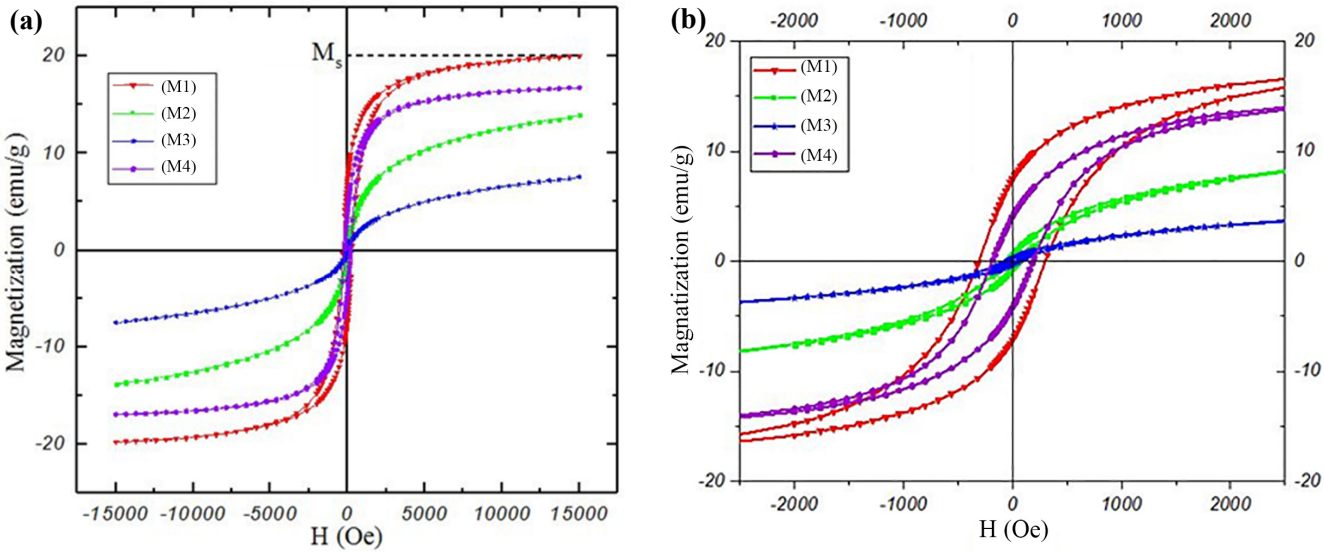

Fig. 8. (a) Magnetic hysteresis loops for M1 to M4 samples and (b) at higher magnification.

samples M2 and M3 (Figs. 8(a) and 8(b)), and the higher crystallinity of M4 led to an increase in coercivity for M4. Similar behavior has been reported by Mozaffari *et al.* for M_s and H_c [23] and also by Ishaque *et al.* [7] for M_s.

4. Conclusions

Nickel ferrite particles were successfully prepared via the co-precipitation synthesis route, and the effect of Y^{3+} ions addition on the structure, molecular, microstructure, and magnetic behavior of particles were studied. The main results can be concluded as follows:

1) $NiFe_2O_4$ with a spinel structure was formed as the dominant phase for all the samples.
2) Adding different amounts of Y^{3+} ions dopant from x = 0 (M1) to x = 0.02 (M2) caused considerable lattice distortion and, consequently, a significant decrease in peak intensities. However, the increase of Y^{3+} ions up to x = 0.12 (M4) led to forming of a minor phase of $FeYO_3$, together with the $NiFe_2O_4$ spinel main phase. Also, lattice distortion occurred when adding Y^{3+} ions up to x = 0.06, decreasing XRD peak intensities.
3) Microstructure studies showed that adding Y^{3+} ions dopant up to x = 0.06 led to a considerable decrease in the particle size of powders, and adding more dopant up to x = 0.12 led to the formation of an amorphous and crystalline phase.
4) Magnetic studies demonstrated that lattice distortion due to the substitution of Y^{3+} ions caused a considerable decrease in coercivity when adding Y^{3+} ions up to x = 0.06. The higher crystallinity of the samples with more Y^{3+} ions (x = 0.12) led to increased coercivity.

Table 2. M_s and H_c values for M1 to M4 samples.

Sample	Y Concentration (x, %)	Formula	M_s (emu.g^{-1})	H_c (Oe)
M1	0.00	$NiFe_2O_4$	19.973	310
M2	0.02	$NiY_{0.04}Fe_{1.96}O_4$	13.904	57
M3	0.06	$NiY_{0.12}Fe_{1.88}O_4$	7.522	51.015
M4	0.12	$NiY_{0.24}Fe_{1.76}O_4$	16.719	184.715

Disclosure statement

No potential conflict of interest was reported by the authors.

Acknowledgement

The authors gratefully acknowledge support from the University of Sistan and Baluchestan, Zahedan, Iran. The authors also thank Prof. Mahdi Shafiee Afarani for useful scientific discussions.

References

[1] Aravind, G., Raghasudha, M., & Ravinder, D. (2015). Electrical transport properties of nanocrystalline Li–Ni ferrites. *J. Materiomics*, *1*(4) 348-356.

[2] Azadmanjiri, J., & Seyyed Ebrahimi, S.A. (2004). Influence of stoichiometry and calcination condition on the microstructure and phase constitution of $NiFe_2O_4$ powders prepared by sol-gel autocombustion method. *Phys. Status Solidi C, 1*(12) 3414 - 3417.

[3] Salavati-Niasari, M., Davar, F., & Mahmoudi, T. (2009). A simple route to synthesize nanocrystalline nickel ferrite ($NiFe_2O_4$) in the presence of octanoic acid as a surfactant, *Polyhedron*, *28*(10) 1455-1458.

[4] Manikandan, V., Mirzaei, A, Vigneselvan, S., Kavita, S., Mane, R.S., Kim, S.S., & Chandrasekaran, J. (2019). Role of ruthenium in the dielectric, magnetic properties of nickel ferrite ($Ru-NiFe_2O_4$) nanoparticles and their application in hydrogen sensors. *ACS Omega*, *4*(7) 12919-12926.

[5] Khan, M.A., Islam, M., Ishaque, M., Rahman, I., Genson, A., & Hampshire S. (2009). Structural and physical properties of Ni–Tb–Fe–O system. *Mater. Charact. 60*(1) 73-78.

[6] Kumbhar, S.S., Mahadik, M., Mohite, V., Hunge, Y., Rajpure, K., & Bhosale, C. (2015). Effect of Ni content on the structural, morphological and magnetic properties of spray deposited Ni–Zn ferrite thin films. *Mater. Res. Bull. 67*, 47-54.

[7] Ishaque, M., Khan, M.A., Ali, I., Khan, H.M., Iqbal, M.A., Islam, M., & Warsi, M.F. (2015). Impacts of yttrium substitution on FMR line-width and magnetic properties of nickel spinel ferrites. *J. Magn. Magn. Mater. 382*, 98-103.

[8] Alves, T.E.P., Pessoni, H.V.S., & Franco, Jr A. (2017). The effect of Y^{3+} substitution on the structural, optical band-gap and magnetic properties of cobalt ferrite nanoparticles. *Phys. Chem. Chem. Phys. 19*(25) 16395-16405.

[9] Azadmanjiri, J., & Seyyed Ebrahimi, S.A. (2006). The effects of pH and citric acid concentration on the characteristics of nanocrystalline $NiFe_2O_4$ powder synthesized by a sol–gel autocombustion method. ISSN 0031-918X, *Phys. Metals Metallogr. 102* (Suppl. 1) S21-S23.

[10] Omidi, S., Davarpanah, A.M., & Abbasian, A.R. (2022). Enhancement of specific surface area of $CoFe_2O_4$ powders synthesized by KCl-assisted solution combustion: Effect of KCl content and initial pH. *Iran. J. Phys. Res. 22*(2), 353-371.

[11] Karoblis, D., Mazeika, K., Raudonis, R., Zarkov, A., & Kareiva, A. (2022). Sol-gel synthesis and characterization of yttrium-doped $MgFe_2O_4$ spinel. *Materials*, *15*(21) 7547.

[12] Yao, H., Ning, X., Zhao, H., Hao, A. & Ismail, M. (2021). Effect of Gd-doping on structural, optical, and magnetic properties of $NiFe_2O_4$ as-prepared thin films via facile sol-gel approach, *ACS Omega*, *6*(9) 6305-6311.

[13] Abdul, H., Thamraa, A., Ghulam, M., Alhossainy, M.H., Laref, A., Khan, A.R., Ali, I., Farid, H.M.T., Ghrib, T., Ejaz, S.R., Khosa, R.Y. (2021). Magnetic, dielectric and structural properties of spinel ferrites synthesized by sol-gel method. *J. Mater. Res. Technol. 11*, 158-169.

[14] Ishaque, M., Islam, M.U., Azhar Khan, M., Rahman I.Z., Genson, A., & Hampshire, S. (2010). Structural, electrical and dielectric properties of yttrium substituted nickel ferrites. *Physica B*, *405*(6) 1532-1540.

[15] Tiwari, R., De, M., Tewari, H.S., & Ghoshal, S.K., (2020). Structural and magnetic properties of tailored $NiFe_2O_4$ nanostructures synthesized using auto-combustion method. *Results Phys. 16*, 102916.

[16] Abdi, Z., Malek Khachatourian, A., & Nemati, A. (2022). Studying the effect of calcination on the optical and magnetic properties of $NiFe_2O_4$@ZnO:Ti nanoparticles. *Adv. Ceram. Prog. 8*(3) 1-7.

[17] Abbasian, A.R., Mahvary, A., & Alirezaei, S. (2021). Salt-assisted solution combustion synthesis of $NiFe_2O_4$: Effect of salt type. *Ceram. Int. 47*(17): 23794-23802.

[18] Paborji, F., Shafiee Afarani, M., Arabi, A.M., & Ghahari, M. (2022). Solution combustion synthesis of $FeCr_2O_4$ powders for pigment applications: Effect of fuel type. *Int. J .Appl. Ceram. Tec. 19*(5) 2406-2418.

[19] Paborji, F., Shafiee Afarani, M., Arabi, A.M., & Ghahari, M. (2023). Synthesis of $(Fe,Cr)_2O_3$ solid solution pigment powders for ink application. *Int. J. Appl. Ceram. Tec.* 20(2) 1154-1166.

[20] Al-Garalleh, G.A., Bsoul, I., Maswadeh, Y., Al-Hwaitat, E., & Mahmood, S.H. (2019). Effects of synthesis route on the structural and magnetic properties of $Sr_{1-x}RE_xFe_{12}O_{19}$ nanocrystalline hexaferrites. *Appl. Phys. A*, *125*, 467.

[21] Sharifitabar, M., Vahdati khaki,J., & Haddad Sabzevar, M. (2014). Effects of Fe additions on self propagating high temperature synthesis characteristics of TiO_2–Al–C system, *Int. J. Refract.*

Met. H. 47, 93-101.

[22] Li, Q., Kartikowati, C.W., Horie, S., Ogi, T., Iwaki, T., & Okuyama, K. (2017). Correlation between particle size/domain structure and magnetic properties of highly crystalline Fe_3O_4 nanoparticles. *Sci. Rep.-UK*, *7*(1) 9894.

[23] Mozaffari, M., Amighian, J., & Tavakoli, R. (2015). The effect of yttrium substitution on the magnetic properties of magnetite nanoparticles. *J. Magn. Magn. Mater. 379*, 208-212.

Additional information

Correspondence and requests for materials should be addressed to A.M. Davarpanah.

HOW TO CITE THIS ARTICLE

Moghaddam, A.A.; Davarpanah, A.M. (2022). Structural and magnetic properties of chemically synthesized yttrium-substituted nickel nanoferrite. *J. Particle Sci. Technol. 8(2) 87-94.*

DOI: 10.22104/JPST.2023.6077.1222

URL: https://jpst.irost.ir/article_1269.html